Synchronization of dissolution and precipitation fronts during infiltration-driven replacement in porous rocks

Paweł Kondratiuk,[1] Hanna Tredak,[1,2] Anthony J.C. Ladd,[3] and Piotr Szymczak[1]

Corresponding author: P. Szymczak, Institute of Theoretical Physics, Faculty of Physics, University of Warsaw, Pasteura 5, 02-093, Warsaw, Poland (piotr.szymczak@fuw.edu.pl)

[1]Institute of Theoretical Physics, Faculty of Physics, University of Warsaw, Pasteura 5, 02-093 Warsaw, Poland

[2]Faculty of Geology, University of Warsaw, Żwirki i Wigury 89, 02-089 Warsaw, Poland

[3]Chemical Engineering Department, University of Florida, Gainesville, FL 32611-6005, USA

Coupled dissolution-precipitation reactions, where two minerals share a common ion, occur frequently in geological replacement; the reactions are driven by an inflow of precipitating secondary ions and an outflow of dissolved primary ions. Although crystallization pressure is frequently invoked to explain volume-preserving replacement, it cannot be operative if the chemical reactions lead to a loss of mineral volume; here the host rock that should confine the precipitating mineral is dissolving faster than the grains are growing. In this paper we propose two chemical mechanisms by which a rapid dissolution front and a slower precipitation front can be synchronized, and volume-for-volume replacement preserved. We analyze these mechanisms within the framework of reactive transport theory and show that morphological features observed in calcite replacement can be correlated with predictions of the models.

1. Introduction

Diagenetic replacement often takes place with a near perfect matching of rock volume and texture [*Lindgren*, 1918], but the mechanism by which the volumetric rates of dissolution and precipitation are equalized remains controversial. Crystallization pressure provides an explanation for volume-preserving replacement without reference to the specifics of the mineral chemistry [*Maliva and Siever*, 1988; *Merino et al.*, 1993; *Minguez and Elorza*, 1994]. For example, if an incoming solution of aqueous ions is oversaturated, then as the replacement mineral precipitates it increases the pressure on the primary mineral in the region where it is growing, shifting the equilibrium in favor of dissolution of the primary mineral. The pressure in the rock increases until the volumetric rates of dissolution and precipitation are equal [*Maliva and Siever*, 1988]. Moreover, if the incoming solution is undersaturated with respect to the host, then it is possible for the dissolving rock to induce precipitation by reducing the pressure in the rock matrix, once again introducing a coupling between the volumetric rates [*Minguez and Elorza*, 1994]. More recently, crystallization pressure has been incorporated into systems where there is a chemical coupling between dissolution and precipitation [*Merino and Banerjee*, 2008]. However, the crystallization pressure model has been criticized [*Putnis*, 2009], in part because many systems exhibit volume-preserving replacement in the absence of confinement. Instead, Putnis proposes a coupled dissolution-precipitation model, emphasizing the role of the fluid layer at the interface between the primary and secondary minerals. During replacement, the composition of this layer can be significantly different from the composition in the bulk fluid and, if the minerals share a common ion, dissolution causes

the interfacial solution to become oversaturated with respect to the secondary mineral. The volume of the precipitate matches the volume of dissolved material through a change in porosity in the replacement phase [*Putnis*, 2009; *Pollok et al.*, 2011].

At the field scale, transport processes, and convective flow in particular, play an important role in the overall reaction rates. In this letter, reactive transport theory is used to analyze infiltration-driven replacement in which there is a common ion shared between the two minerals; examples include clay-for-calcite replacement [*Merino and Banerjee*, 2008], dolomitization [*Merino and Canals*, 2011], and serpentinization [*Beinlich et al.*, 2012]. Going beyond the pioneering work of [*Korzhinskii*, 1968], who assumed volume-for-volume replacement from the outset, we establish conditions under which the volumetric rates of precipitation and dissolution can be balanced. We focus on cases where the solution chemistry leads to a loss of molar volume during replacement, so that there is no means for the growing crystal to exert pressure on the surrounding grains. Even if a local increase in pressure is postulated, it will only make the volume mismatch larger. Thus we can eliminate crystallization pressure as a candidate mechanism for volume preservation in these systems.

We have investigated two chemical coupling mechanisms that can reduce the volumetric rate of dissolution during replacement. One way is if the incoming solution is in equilibrium with the secondary mineral (Sec. 3). When this solution encounters the primary mineral, its equilibrium shifts and secondary mineral is then precipitated. However, if the dissolution front runs away from the precipitation front the original equilibrium is restored and precipitation stops. This is a self-regulating process, leading to a steadily

propagating replacement front over a range of solution parameters.The excess volume is taken up through an increase in porosity in the replacement phase, similar to observations in a number of laboratory experiments [*Putnis*, 2009].

On the other hand, if the incoming solution is oversaturated with respect to the secondary mineral, the dissolution front will run ahead of precipitation because there is now no means to prevent the continued production of the aqueous ions, typically protons, that dissolve the primary mineral. For oversaturated inlet solutions, we propose a different mechanism to synchronize the fronts, which includes a competing reaction to soak up the excess protons (Sec. 4). Buffering anions can lead to a steadily-propagating interfacial region, with a narrow band of high porosity between two compact mineral phases. The thickness of the porous band depends on the relative rates of precipitation and buffering and can expand or contract to accommodate changes in chemical composition.

These two replacement mechanisms differ from observations in the laboratory, where there is no flow and ion transport is purely diffusional [*Putnis and Putnis*, 2007; *Putnis*, 2009; *Pollok et al.*, 2011]. However, in geological systems replacement is always dominated by convection; even over time scales of millions of years, aqueous ions can only be transported over distances of ~ 100m by diffusion. Given the difference between ion concentrations in solution and in minerals (ratios of $10^{-5} - 10^{-6}$), replacement bands would be limited to thicknesses of the order of $1 - 10$cm in the absence of convection.

This work comprises analytic solutions for steadily propagating replacement fronts and numerical simulations of the approach to steady state. We have verified that the mechanisms discussed in Secs. 3 and 4 lead to steady replacement fronts with exact volume

matching between primary and secondary mineral phases. We compare predictions from the model systems with examples of calcite replacement. Several morphological features observed in the field can be identified with predictions of the models. The main results are reported in the body of the letter, while technical details, together with additional numerical examples, are contained in the Supplementary Materials.

2. Front synchronization: a condition for volume-preserving replacement

Figure 1 illustrates the geometry of a model replacement process, characterized by a planar reaction front and a one-dimensional flow with Darcy velocity v_0. An aqueous solution of secondary ions A_S infiltrates a porous matrix of the primary mineral M_P, precipitating the secondary mineral M_S and releasing aqueous protons (or other coupling species) X, which in turn dissolve the primary mineral with release of ions A_P. We represent the chemistry of the precipitation and dissolution by the following schematic reactions:

$$A_S \longleftrightarrow M_S + \nu X, \tag{1}$$

$$X + M_P \longrightarrow A_P. \tag{2}$$

We assume that regions far from the front contain only a single solid component, either the original mineral M_P with a volume fraction ϕ_P^{max} ($x \to +\infty$) or the replacement mineral M_S with a volume fraction ϕ_S^{max} ($x \to -\infty$). We have assumed that the dissolution reaction (2) is irreversible so that the concentration of secondary ions and protons vanishes at the outlet; this simplifies the calculations without affecting the conclusions. In general, the precipitation front (the rightmost point where $\phi_S = \phi_S^{max}$) and the dissolution front (the rightmost place where $\phi_P = 0$) will move at different speeds [*Ortoleva et al.*, 1986;

Lake et al., 2002], as indicated in Fig. 1. In this section we derive a condition to equalize the front velocities, and therefore generate a volume preserving replacement.

The stoichiometric volume ratio [*Pollok et al.*, 2011] of reactions (1) and (2) is

$$\Delta_{crys} = \frac{c_P^{sol}}{\nu c_S^{sol}}, \tag{3}$$

where c_P^{sol} and c_S^{sol} are the molar concentrations (per liter) of the minerals. A molar volume preserving replacement is characterized by $\Delta_{crys} = 1$, but most replacement reactions are accompanied by a reduction in volume ($\Delta_{crys} < 1$) [*Putnis*, 2009], although there are cases where the molar volume increases [*Putnis and Putnis*, 2007]. The stoichiometry of the overall replacement reaction,

$$\nu M_P + A_S \longleftrightarrow M_S + \nu A_P, \tag{4}$$

depends on the relative solubility of the minerals [*Pollok et al.*, 2011] and the concentration of secondary ions in the inlet stream. We will therefore treat the stoichiometry number ν as an independent parameter, not one that can be regulated to create the conditions for a constant volume replacement.

The speed of a steady precipitation front can be found by matching the incoming flux of aqueous ions, $v_0 c_S^{in}$ to the rate at which the rock volume is consumed $U_{prec} c_S^{sol} \phi_S^{max}$; here U_{prec} is the front velocity and ϕ_S^{max} is the mineral volume fraction in the fully precipitated rock. The front velocity is determined by the molar volume of the rock $(c_S^{sol}\phi_S^{max})^{-1}$, rather than the molar volume of the mineral $(c_S^{sol})^{-1}$, and is *independent of the reaction kinetics*. Applying a similar reasoning to the dissolution front:

$$U_{prec} = \frac{v_0 c_S^{in}}{c_S^{sol}\phi_S^{max}}, \qquad U_{diss} = \frac{v_0 c_P^{out}}{c_P^{sol}\phi_P^{max}}, \tag{5}$$

where c_P^{out} is the concentration of aqueous ions at the outlet. The formulas are simplified by the assumption of irreversible dissolution, which means that there are no secondary ions in the output stream; we have also assumed there are no primary ions in the inlet stream. Matching the front velocities, $U_{diss} = U_{prec}$, gives a general condition for constant rock volume replacement, which for the chemistry outlined in reactions (1) and (2) reduces to

$$c_P^{out} = \nu c_S^{in} \Delta, \tag{6}$$

where

$$\Delta = \frac{c_P^{sol} \phi_P^{max}}{\nu c_S^{sol} \phi_S^{max}} \tag{7}$$

is the counterpart of Δ_{crys}, but for rock volumes. Note that the condition for a volume preserving replacement (6) is not $\Delta = 1$, which one might be expected from purely volumetric considerations, although it reduces to it for an irreversible precipitation reaction (see Sec. 3). In the next two sections we consider how Eq. (6) can be satisfied in replacement processes where crystallization pressure is not operative.

3. Equilibrium mechanism: Inlet stream is saturated with respect to the secondary mineral

An oversaturated solution at the inlet, as envisaged by *Korzhinskii* [1968] and *Banerjee and Merino* [2011], forces continued precipitation until the pore space in the replacement phase is filled. At this point, if replacement is accompanied by loss of molar volume ($\Delta_{crys} < 1$), a larger volume of primary mineral has dissolved, leaving an empty space between the two phases that grows with time. However, if the incoming solution is saturated rather than oversaturated, precipitation ceases in regions where there is no

primary mineral to absorb the protons; now the dissolution front can no longer run ahead of precipitation. The loss of molar volume is compensated by an increase in porosity in the replacement phase so that the mineral volume remains the same. In this section we analyze the condition for volume preserving replacement, given by Eq. (6), when the inlet solution is in equilibrium with the secondary mineral; $c_S^{in} = K_S(c_X^{in})^\nu$, and $c_P^{in} = 0$.

A mass balance on the protons entering and leaving the system, $c_X^{in} + \nu c_S^{in} - c_P^{out} = 0$, connects the volume change Δ in Eq. (6) to the dissolution constant of the secondary mineral $K_S = c_S^{in}/(c_X^{in})^\nu$ (1);

$$\Delta = 1 + \nu^{-1}C, \tag{8}$$

where the dimensionless concentration at the inlet $C = c_X^{in}/c_S^{in} = [K_S(c_S^{in})^{\nu-1}]^{-1/\nu}$. The flexibility needed to synchronize the fronts comes from an increase in the porosity of the replacement mineral, as is frequently observed experimentally [*Putnis*, 2009]. The porosity automatically adapts to the change in molar volume and the equilibrium at the inlet; combining Eqs. (6) and (8) gives the volume fraction of the replacement phase as

$$\phi_S^{max} = \frac{\phi_P^{max}\Delta_{crys}}{1 + \nu^{-1}C}. \tag{9}$$

The replacement mineral faction (ϕ_S^{max}) is always less than that suggested by the condition $\Delta = 1$, which is only achieved in the limit $K_S \to \infty$ (8). A more general condition for volume-preserving replacement, can be found in fronts.pdf (Supplementary Materials).

An equilibrium condition at the inlet leads to a more porous replacement phase when $\Delta_{crys} < 1$, as illustrated in the top panel of Fig. 2. The key parameters, $\nu = 1$, $\Delta_{crys} = 0.7$ and $K_S = 9$, were chosen to represent a substantial (30%) loss of molar volume and a solubility of the replacement mineral of 10^{-5}M at pH $\approx$ 6. The replacement

mineral porosity is then large (43%), but similar to experimental results for KCl−NaCl replacement (for instance), where a homogeneous distribution of porosity was observed [*Pollok et al.*, 2011]. The corresponding concentration profiles are shown in Supplementary Fig. 1, while the development of invariant profiles from a homogeneous initial condition, using the parameters indicated in Fig. 2 (Top), is shown in movie1.avi.

The mineral profiles in Fig. 2 were obtained with linear reaction kinetics ($\nu = 1$),

$$r_{prec} = k_{prec}(c_S - K_S c_X), \quad r_{diss} = k_{diss} c_X. \tag{10}$$

With the assumption that dissolution is faster than precipitation ($k_{diss} \gg k_{prec}$), the characteristic length scale is that of the precipitation front

$$l_{prec} = \frac{2D}{v_0(\sqrt{1+4H}-1)}; \tag{11}$$

the dimensionless parameter $H = Dk_{prec}/v_0^2$ [*Szymczak and Ladd*, 2013], where $D = D_{mol}\phi$ is the dispersion coefficient, the product of molecular diffusion and porosity, which we assume to be constant.

Interestingly, the equilibrium model not only predicts constant-volume replacement with a sharp interface between the two minerals, but it gives a mechanism for texture preservation as well. We find that regions of higher mineral volume fraction in the primary phase are replaced by corresponding regions of increased secondary mineral content; closely coupled variations in volume fraction after replacement can be seen in movie2.avi (Supplementary Materials).

4. Buffering mechanism: Dissolution is suppressed by a competing reaction

137 It seems likely that geological replacement is sometimes driven by oversaturated solu-
138 tions of the incoming ions; if so, a different coupling mechanism from the one described in
139 Sec. 3 is needed to preserve rock volume. In this case the replacement mineral will con-
140 tinue to precipitate until it fills all the available pore space, but once again, crystallization
141 pressure [*Maliva and Siever*, 1988; *Merino and Banerjee*, 2008] is unable to synchronize
142 the fronts when the volumetric rate of precipitation is larger than the volumetric rate of
143 dissolution [*Putnis*, 2009].

An alternative mechanism for front synchronization is suggested by the observation that dissolution is controlled by the number of protons generated in the precipitation reaction (2). By introducing a competing reaction,

$$B + X \longrightarrow BX, \tag{12}$$

which depletes the concentration of protons in the zone between the fronts (the white region in Fig. 1), the dissolution front becomes synchronized with the precipitation front ($U_{diss} = U_{prec}$) over a distance δ. Our analysis uses irreversible kinetics for the mineral reactions (Eq. (10) with $K_S = 0$) as well as an irreversible buffering reaction

$$r_{buff} = k_{buff} c_X, \tag{13}$$

144 in effect assuming a large excess of anions (B). The qualitative features of the replacement
145 front are insensitive to the form of the reaction kinetics; they depend mainly on the non-
146 dimensional numbers Δ and H, and ratios of the rate constants.

The case of weak buffering, meaning $k_{buff} \ll v_0^2/D \ll k_{prec} \ll k_{diss}$, offers a physical picture of how a buffering reaction synchronizes the fronts. The concentration of protons decreases exponentially from the precipitation front x_S, with a convective length scale

v_0/k_{buff} [*Szymczak and Ladd*, 2013],

$$c_X(x) = c_X(x_S)e^{-k_{buff}(x-x_S)/v_0}. \tag{14}$$

The proton concentrations at the two front positions, x_S and x_P, are determined by mass balances (since the buffering is slow): $c_X(x_S) = \nu c_S^{in}$ and $c_X(x_P) = c_P^{out} = \nu c_S^{in}\Delta$. There is then a single location $x_P = x_S + \delta$, where the concentration of protons reaches the level required to synchronize the dissolution front to the precipitation reaction (6),

$$\delta = \frac{v_0}{k_{buff}} \ln \Delta^{-1}. \tag{15}$$

Remarkably, this mechanism leads to a *stable* synchronization of the fronts: a small decrease in the distance between the fronts results in an effective increase of c_X at the dissolution front and an increase in its velocity. Conversely, an increase in δ results in a slowdown of the dissolution front. Thus the fronts remain synchronized even with an oversaturated solution at the inlet.

The width of the zone separating the two fronts, $\delta = x_P - x_S$, decreases with increasing buffering rate; this is a self-regulatory process, which assures the correct concentration of protons at the dissolution front over a wide range of k_{buff}. It is commonly the case that the buffering reaction is faster than precipitation, in which case the scale of the replacement front is l_{prec} (16) and

$$\delta = l_{prec} \ln \Delta^{-1}. \tag{16}$$

The bottom panel of Fig. 2 shows steady-state mineral profiles for buffered replacement; the corresponding concentration profiles can be found in Supplementary Fig. 2. The development of a time-invariant front from a uniform initial condition is shown in

movie3.avi (Supplementary Materials). The dissolution front, which in the absence of the buffering reaction would advance with a different velocity U_{diss} (5), is now synchronized with the precipitation front.

There is a wave of excess porosity between the two fronts (bottom panel of Fig. 2), which reaches its maximum value,

$$\phi^{max} = 1 - \phi_S^{max} \exp(-\delta/l_{prec}), \tag{17}$$

at the dissolution front ($x = x_P$). When buffering is slow (15), $\delta \gg l_{prec}$ and the intermediate region is highly porous; for fast buffering (16), $\phi^{max} = 1 - \phi_S^{max}\Delta$.

An exact synchronization of the front velocities requires a strictly irreversible buffering reaction (12). Nevertheless the fronts will remain closely coupled as long as the rate of acid dissociation is much less than the rate of buffering.

5. Application of the equilibrium mechanism: Replacement of calcite by dolomite

Merino and Canals [2011] consider dolomitization to be an example of crystallization pressure leading to constant-volume replacement. In their view, volume and texture preservation cannot be explained by a dissolution-precipitation mechanism. However, we will argue that when the incoming solution is undersaturated with respect to both minerals, the fronts become synchronized through the equilibrium mechanism outlined in Sec. 3.

When the solution entering the primary rock is undersaturated with respect to both calcite and dolomite, the calcite near the inlet dissolves, raising the saturation indexes of both calcite and dolomite. If the dolomite solution saturates first, it begins to precipitate

as illustrated by the sketch in the supplementary document fronts.pdf (Supplementary Materials). Once dolomite saturation is reached, the pure dissolution front gives way to a dissolution-precipitation front, which remains sharp because the solution to the left of the front is in equilibrium with the secondary mineral (Sec. 3). Assuming the dolomite dissolution front is slower than the dissolution-precipitation front, the band of dolomite grows with time.

We used PHREEQC [*Parkhurst and Appelo*, 2013] to determine the change in molar volume for input solutions containing varying concentrations of aqueous Mg^{2+}, Ca^{2+} and dissolved carbon; a summary of these calculations is given in Table I of fronts.pdf (Supplementary Materials). We included simplified versions of the brine models used by *Merino and Canals* [2011] but in all cases we found that undersaturated solutions lead to near stoichiometric replacement thermodynamically, with 1 mole of dolomite replacing almost exactly 2 moles of calcite, for a net loss in molar volume of 13%. In some cases, for instance when the concentrations of calcium and magnesium ions are small, the volume loss can be larger, up to about 25%, but never less than 13%. This would seem to rule out crystallization pressure as a synchronization mechanism for dolomitization at least when the incoming solution is undersaturated with respect to dolomite.

The assumption that dolomite precipitation only occurs when the incoming solution reaches saturation (from calcite dissolution), rather than being oversaturated from the outset means that velocities of the dissolution and precipitation are equal (Sec. 2), and the front separating the dolomite and calcite regions does not spread in time. Dolomite precipitation rates measured in the laboratory [*Arvidson and Mackenzie*, 1999] were typ-

ically around $10^{-12}\mathrm{Mcm}^{-2}\mathrm{s}^{-1}$ with solution concentrations of the order of 10mM, which suggests a characteristic rate $k_{prec} \sim 10^{-5}\mathrm{s}^{-1}$, taking the reactive surface area as $100\mathrm{cm}^{-1}$. With a fluid flow velocity in the range from $10^{-7} - 10^{-6}\mathrm{cm\,s}^{-1}$ (or $3 - 30$ $\mathrm{cm\,yr}^{-1}$), the predicted front thickness is $3 - 4$mm.

6. Application of the buffering mechanism: Replacement of calcite by kaolinite

Clay-precipitation is a classical example of an acid-producing (or "reverse weathering") reaction [*Mackenzie*, 2005]. If this process takes place in the vicinity of carbonate rocks, then the coupling between dissolution and precipitation described by Eqs. (1)-(2) can arise, as has been hypothesized previously [*Frolking et al.*, 1983; *Lijun and Jingyang*, 2002; *Lucke et al.*, 2012]. For example, if the precipitating clay is kaolinite [*Merino and Banerjee*, 2008], the reactions are:

$$\mathrm{Al}^{3+} + \mathrm{H_4SiO_4} + \frac{1}{2}\mathrm{H_2O} \rightarrow \frac{1}{2}\mathrm{Al_2Si_2O_5(OH)_4} + 3\,\mathrm{H}^{+}, \tag{18}$$

$$\mathrm{CaCO_3} + \mathrm{H}^{+} \longrightarrow \mathrm{Ca}^{2+} + \mathrm{HCO_3^{-}}. \tag{19}$$

There is increasing field evidence that carbonate-for-clay replacement is volume preserving. *Frolking et al.* [1983] reported undisturbed chertlines extending from dolomite through the overlaying clays, while *Lijun and Jingyang* [2002] observed that illite covered limestone maintains the micro-bedding structure of the primary rock. Field evidence is supported by textural analysis, which shows that morphological details of the limestone are preserved by the replacing clay minerals [*Lijun and Jingyang*, 2002; *Merino and Banerjee*, 2008; *Lucke et al.*, 2012].

While modeling the formation of terra rossa, *Banerjee and Merino* [2011] assumed that the incoming solution is supersaturated with respect to kaolinite, which is consistent

with observations that significant kaolinite supersaturation can occur at pH > 4 [*Yang and Steefel*, 2008]. Since the solubility of silica is relatively high (in the $100\,\mu$M range), precipitation is likely to be limited by the Al^{3+} concentration, and we will assume a linear dependence of r_{prec} on the aluminum concentration, $c_S = [Al^{3+}]$, as in Eq. (10) (with $K_S = 0$). In order to approximate the precipitation rates reported in *Yang and Steefel* [2008] with an incoming aluminum concentration of 10^{-5} M [*Banerjee and Merino*, 2011], we need a rate constant of approximately $6 \times 10^{-10}\mathrm{cm\,s^{-1}}$. Taking the reactive surface area in the range $100 - 200\mathrm{cm^{-1}}$ leads to a value for k_{prec} (10) of the order of $10^{-7}\mathrm{s^{-1}}$. The dissolution of calcite [*Cubillas et al.*, 2005] is 7–9 orders of magnitude faster than the precipitation of kaolinite, and we take $k_{diss} = 10^8 k_{prec}$.

These reactions cannot lead to a steadily propagating replacement front when the incoming solution is oversaturated (Sec. 2). However, the field observations imply a tight coupling between the precipitation and dissolution, with an intermediate zone that is just a few cm wide, compared to $1 - 5\,$m of precipitated clay; this suggests that U_{diss} and U_{prec} must be synchronized to within a few percent. We have therefore extended the model from *Banerjee and Merino* [2011], by taking into consideration the buffering of H^+ ions by bicarbonate anions:

$$H^+ + HCO_3^- \longrightarrow H_2CO_3. \tag{20}$$

This leads to the situation described by the buffering model (Sec. 4).

Most terra rossa formations are found in neutral soils, implying that the dissolved CO_2 has been neutralized by sub-surface flow through the surrounding calcite. This would require almost complete dissociation of the dissolved CO_2 and conversion of the protons to

calcium and bicarbonate ions. Thus we will assume that our input solution is composed of calcium and bicarbonate ions, in addition to Al^{3+} and H_4SiO_4. The buffering reaction can then be treated as irreversible, with a rate $r_{buff} = k_2[H^+][HCO_3^-]$, where $k_2 \sim 10^5\,M^{-1}s^{-1}$ [*Ho and Sturtevant*, 1963]. We take the bicarbonate ion concentration as 10^{-5}M; since $[HCO_3^-]$ is in excess, the kinetics are roughly linear in the proton concentration $r_{buff} = k_{buff}[H^+]$, with $k_{buff} \sim 1\,s^{-1}$.

The kinetics data must be supplemented with values for the transport parameters. Assuming annual rainfall of the order of 1 m/yr [*Banerjee and Merino*, 2011], the Darcy velocity is of the order of 10^{-6}cm s^{-1}, while the dispersion constant $D \approx 10^{-6}$cm^2 s^{-1}. These choices result in a dimensionless transport parameter $H = 0.1$. We assume a porosity of 25% in both the calcite ($\phi_P^{max} = 0.75$) and in the precipitated kaolinite ($\phi_S^{max} = 0.75$). The molar volumes of calcite and kaolinite, together with the stoichiometry number $\nu = 3$, lead to $\Delta \approx 0.45$. The mineral and concentration profiles for these parameters are shown in Supplementary Fig. 3. The protons produced by kaolinite precipitation are consumed immediately, either by dissolving calcite or by buffering; thus the only length scale derives from the precipitation front, $l_{prec} \approx 9$ cm.

The results show several points of agreement with observations of calcite replacement by kaolinite [*Banerjee and Merino*, 2011]. There is a small separation of the fronts (of the order of centimeters) in comparison with the distance traveled (meters); this synchronization results from a purely chemical coupling of precipitation and dissolution by the irreversible buffering reaction. Consistent with field observations, the model predicts a 10 cm bleached zone of enhanced porosity ($\phi^{max} \approx 0.6$) in between the fronts.

7. Summary

In this paper, we have explored chemical mechanisms by which a tight coupling between precipitation and dissolution fronts can arise, leading to volume-preserving replacement. Standard models of infiltration-driven replacement [*Korzhinskii*, 1968] implicitly assume volume preservation, but the mechanisms by which it comes about have not been fully elucidated. There are a number of commonly occurring replacements where crystallization pressure cannot synchronize the fronts [*Putnis*, 2009], and in this letter two chemical mechanisms have been proposed that can operate when replacement involves a loss of mineral volume.

In the first mechanism, additional porosity is generated in the secondary phase, with the amount of new porosity adjusting itself to the value needed for front synchronization. In the second model, synchronization is accomplished by a buffering reaction which reduces the concentration of coupling ions to a value that allows for the front velocities to match. Both processes are self-regulating, allowing for stable, volume preserving fronts to propagate. The first mechanism is applicable to situations where the inlet solution is saturated (or slightly undersaturated) whereas the second mechanism can allow for volume-preserving replacement even when the inlet solution is oversaturated. By assuming linear kinetics, we were able to derive analytic expressions for the mineral profiles, and relate some of their characteristic features to natural systems where limestone is replaced by dolomite or authigenic clay.

Although geological systems are characterized by more complex chemical reactions than those considered here, the overall mechanisms of front synchronization should still be

operative. In this paper we have sought to present the key ideas in the simplest possible framework; the condition for volume preserving replacement given in Eq. (6) is specific to the reactions (1) and (2), but similar conditions can be derived for more complex chemistry (see fronts.pdf in the Supplementary Materials). For example, whenever there is a buffering reaction (or reactions) reducing the concentration of the coupling ions, then the distance between the fronts will become stabilized by a feedback loop at a value which guarantees an exact matching of the dissolved and precipitated volumes. Although the details of the mineral profiles are hard to establish without a detailed knowledge of the chemical kinetics, they should share some general features, such as the presence of a high porosity region at the interface between the primary and secondary minerals, which is indeed observed across a variety of systems [*Merino and Banerjee*, 2008; *Plan et al.*, 2012].

Acknowledgments. We thank Prof. E. Merino (Indiana University) for drawing our attention to this problem. This material is based upon work supported by the National Science Center (Poland) under research Grant No. 2012/07/E/ST3/01734 and by the U.S. Department of Energy Office of Science, Office of Basic Energy Sciences under Award Number DE-FG02-98ER14853. Paweł Kondratiuk is a beneficiary of the project "Scholarships for PhD students of Podlaskie Voivodeship" co-financed by the European Social Fund, the Polish Government and Podlaskie Voivodeship.

The results presented in this letter are based on derivations and calculations given in the Supplementary Materials. Additional parameter values can be investigated interactively using the Computable Document Format (.cdf) files. They require the CDF player, which

can be downloaded from http://www.wolfram.com/cdf-player. Complete formulas are available in the Mathematica^{TM} notebooks (.nb files).

References

Arvidson, R. S., and F. T. Mackenzie (1999), The dolomite problem: Control of precipitation kinetics by temperature and saturation state, *Am. J. Science*, *299*(4), 257–288.

Banerjee, A., and E. Merino (2011), Terra Rossa Genesis by Replacement of Limestone by Kaolinite. III. Dynamic Quantitative Model, *J. Geol.*, *119*(3), 259–274.

Beinlich, A., O. Plümper, J. Hövelmann, H. Austrheim, and B. Jamtveit (2012), Massive serpentinite carbonation at Linnajavri, N-Norway, *Terra Nova*, *24*(6), 446–455, doi: 10.1111/j.1365-3121.2012.01083.x.

Cubillas, P., S. Köhler, M. Prieto, C. Chaïrat, and E. H. Oelkers (2005), Experimental determination of the dissolution rates of calcite, aragonite, and bivalves, *Chemical Geology*, *216*(1-2), 59–77, doi:10.1016/j.chemgeo.2004.11.009.

Frolking, T., M. Jackson, and J. Knox (1983), Origin of red clay over dolomite in the loess-covered Wisconsin driftless uplands, *Soil Sci. Soc. Am. J.*, *47*(4), 817–820.

Ho, C., and J. M. Sturtevant (1963), The Kinetics of the Hydration of Carbon Dioxide at 25°C, *The Journal of Biological Chemistry*, *238*, 3499–3501.

Korzhinskii, D. S. (1968), The theory of metasomatic zoning, *Miner. Deposita*, *231*, 222–231.

Lake, L., S. Bryant, and A. Araque-Martinez (2002), *Geochemistry and Fluid Flow*, Elsevier.

Lijun, Z., and L. Jingyang (2002), Metasomatic mechanism of weathering-pedogenesis of carbonate rocks: I. Mineralogical and micro-textural evidence, *Chin. J. Geochem.*, *21*(4), 334–339.

Lindgren, W. (1918), Volume Changes in Metamorphism, *J. Geol.*, *26*(6), 542–554.

Lucke, B., H. Kemnitz, and R. Bäumler (2012), Evidence for isovolumetric replacement in some Terra Rossa profiles of northern Jordan, *Boletin de la Sociedad Geológica Mexicana*, *64*(1), 21–35.

Mackenzie, F. T. (2005), *Sediments, diagenesis, and sedimentary rocks: treatise on geochemistry*, vol. 7, Elsevier.

Maliva, R. G., and R. Siever (1988), Diagenetic replacement controlled by force of crystallization, *Geology*, *16*, 688–691.

Merino, E., and A. Banerjee (2008), Terra Rossa genesis, implications for Karst, and Eolian dust: A geodynamic thread, *J. Geol.*, *116*, 62–75.

Merino, E., and A. Canals (2011), Self-accelerating dolomite-for-calcite replacement: Self-organized dynamics of burial dolomitization and associated mineralization, *Am. J. Sci.*, *311*, 572–607.

Merino, E., D. Nahon, and Y. Wang (1993), Kinetics and mass transfer of pseudomorphic replacement; application to replacement of parent minerals and kaolinite by Al, Fe, and Mn oxides during weathering, *Am. J. Sci.*, *293*, 135–155, doi:10.2475/ajs.293.2.135.

Minguez, J. M., and J. Elorza (1994), Diagenetic volume-for-volume replacement: force of crystallization and depression of dissolution, *Mineral. Mag.*, *58*, 135–142.

Ortoleva, P., G. Auchmuty, J. Chadam, J. Hettmer, E. Merino, C. Moore, and E. Ripley (1986), Redox front propagation and banding modalities, *Physica D*, *19*(3), 334–354, doi:10.1016/0167-2789(86)90063-1.

Parkhurst, D. L., and C. A. J. Appelo (2013), Description of input and examples for PHREEQC version 3–a computer program for speciation, batch- reaction, one-dimensional transport, and inverse geochemical calculations., *Tech. rep.*, U.S. Geological Survey: http://pubs.usgs.gov/tm/06/a43.

Plan, L., C. Tschegg, J. D. Waele, and C. Spötl (2012), Corrosion morphology and cave wall alteration in an Alpine sulfuric acid cave (Kraushöhle, Austria), *Geomorphology*, *169-170*, 45–54.

Pollok, K., C. V. Putnis, and A. Putnis (2011), Mineral replacement reactions in solid solution-aqueous solution systems: volume changes, reactions paths and end-points using the example of model salt systems, *Amer. J. Sci.*, *311*, 211–236.

Putnis, A. (2009), Mineral Replacement Reactions, *Rev. Mineral. Geochemistry*, *70*(1), 87–124, doi:10.2138/rmg.2009.70.3.

Putnis, A., and C. V. Putnis (2007), The mechanism of reequilibration of solids in the presence of a fluid phase, *J. Solid State Chem.*, *180*(5), 1783–1786, doi: 10.1016/j.jssc.2007.03.023.

Szymczak, P., and A. J. C. Ladd (2013), Interacting length scales in the reactive-infiltration instability, *Geophys. Res. Lett.*, *40*, 3036–3041, doi:10.1002/grl.50564.

Yang, L., and C. I. Steefel (2008), Kaolinite dissolution and precipitation kinetics at 22°C and pH 4, *Geochimica et Cosmochimica Acta*, *72*(1), 99–116, doi:

349 10.1016/j.gca.2007.10.011.

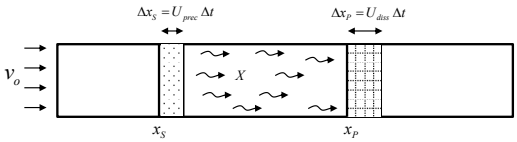

Figure 1. Schematic of a precipitation-dissolution system. The sketch shows a precipitating secondary front (left) gradually replacing the primary mineral (right). In general, the distance between the two fronts $x_P - x_S$ is time varying, as indicated here.

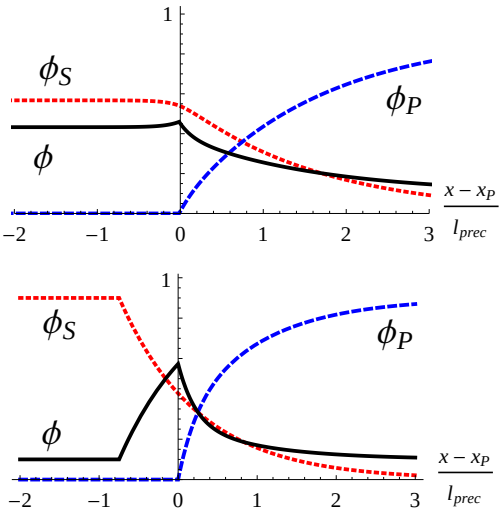

Figure 2. Mineral profiles for steady-state replacement. Volume fractions of primary mineral (blue dashed), secondary mineral (red dotted), and porosity (black solid) are shown in a frame advancing with a constant velocity $U = U_{prec}$. The x-axis is scaled by the characteristic length l_{prec} (11) and has its origin at the position of the dissolution front x_P. Top: mineral profiles from the equilibrium model with $K_S = c_S^{in}/c_X^{in} = 9$ and $\Delta_{crys} = 0.7$. The porosity of the replacement mineral $1 - \phi_S^{max} = 0.433$ (8). Bottom: mineral profiles from the buffering model with $k_{buff}/k_{prec} = 1$ and $\phi_S^{max} = 0.9$. The arrow marks the position of the precipitation front. The common input parameters for both models are: $\nu = 1$, $\Delta_{crys} = 0.7$, $\phi_P^{max} = 0.9$, $k_{diss}/k_{prec} = 10$, and $H \equiv Dk_{prec}/v_0^2 = 1$.